Evaporation-driven growth of large crystallized salt structures in a porous medium

N. Sghaier,[1] S. Geoffroy,[2] M. Prat,[3,*] H. Eloukabi,[1] and S. Ben Nasrallah[1]

[1]*Laboratoire d'Etudes des Systèmes Thermiques et Energétiques de Monastir, Tunisia*

[2]*Université de Toulouse, UPS, INSA, LMDC (Laboratoire Matériaux et Durabilité des Constructions), 135, Avenue de Rangueil, F-31077 Toulouse Cedex 04, France*

[3]*Université de Toulouse, INPT, UPS, IMFT, Avenue Camille Soula, F-31400 Toulouse, France and CNRS, IMFT, F-31400 Toulouse, France*

Subflorescence refers to crystallized salt structures that form inside a porous medium. We report a drying experiment revealing major development of subflorescence in the dry region of the porous medium away from the liquid zone. Using a combination of image analyses and numerical computations, we show that the growth is directly correlated to the evaporation flux distribution along the boundary of the growing salt structure. This indicates that the salt is transported into the domain occupied by the salt structure in the porous medium up to the structure periphery, where salt deposition takes place. This is confirmed when a growing salt structure encounters dry subflorescence formed earlier during the drying process. The dry subflorescence is reimbibed and resumes its growth. The analysis also suggests that the solution within the growing subflorescence is in equilibrium with the crystallized salt wall. These results shed light on the growth mechanisms of subflorescence, a phenomenon that can play a fundamental role in several important issues such as carbon dioxide sequestration or salt weathering.

PACS number(s): 81.10.−h, 47.56.+r

I. INTRODUCTION

Salt crystallization induced by evaporation is an important issue in relation with several domains, such as soil physics [1], the underground sequestration of CO_2 [2], and salt weathering, i.e., the attack of rock and building materials by salt [3]. It is now widely accepted that the crystallization process can induce sufficient stresses on pore walls to cause major damage to porous materials, e.g., [4]. As discussed in [5], the crystallized salt structures forming at the surface of a porous medium are referred to as *efflorescence* whereas the crystallized salt structures forming inside a porous material are referred to as *subflorescence*. Subflorescence is potentially the more damaging phenomenon since it corresponds to crystallization inside internal pores. While the analysis of the interplay between evaporation and efflorescence development has been the subject of several studies in recent years, e.g., [5–10], the understanding of subflorescence development within a porous material is much less advanced.

A better understanding is proposed in this paper, through a simple evaporation experiment allowing the growth of subflorescence to be directly observed.

II. EXPERIMENTAL SETUP

The two-dimensional transparent model porous medium considered in this study consisted of a monolayer of 1-mm-diameter glass beads. The beads were randomly thrown onto a glass plate coated with a hydrophobic sticky film. After removal of the excess beads, a second glass plate was put on top of the bead monolayer. In order to obtain a hydrophobic model, the glass beads and the glass plates were rendered hydrophobic by silanization, a process that leads to a contact angle of about 107°–110° regardless of the NaCl concentration [11]. Three

lateral edges were sealed with RTV (a hydrophobic silicone elastomer) so that the vapor could escape only through the remaining open top edge of the model. The motivation for considering a hydrophobic model was twofold: (i) to obtain a particularly simple drying pattern (an almost flat liquid-gas front) and (ii) to limit the influence of secondary capillary liquid films, e.g., [12], that would make the analysis more complicated. However, subflorescence patterns and growth mechanisms similar to those reported here have been observed in hydrophilic models [13]. Thus the main results concerning the growth of subflorescence reported in this paper are general and not specific to hydrophobic systems. The model was initially fully saturated up to level $z = H$ (see Fig. 1) with a NaCl aqueous solution of known initial concentration $C_0 = 25 \, \text{g}/100 \, \text{g}$ solution. As can be seen from Fig. 1, an additional hydrophobic layer similar to the main micromodel was placed on top of the model. This 10-mm layer did not contain any liquid when the experiment started. It introduced an additional mass transfer resistance (water transport occurred by vapor diffusion in this layer), which limited the evaporation rate and prevented the formation of efflorescence (see [5,10] and references therein for the factors controlling the formation of efflorescence).

The 7-cm-high and 9.5-cm-wide porous medium was placed vertically in a small, transparent Plexiglas chamber at controlled temperature (22 ± 1 °C). The relative humidity in the chamber was stabilized using a saturated LiCl solution [relative humidity (RH) = 12%]. The relative humidity and temperature near the open edge of the model were recorded during the experiments using a sensor (Kimo VT300) connected to a PC and no noticeable evolution was observed. Variation of the model weight during drying was measured with a precision (0.01 g) scale, which was connected to the PC, while the phase distribution within the porous medium was recorded by a charge-coupled device (CCD) camera set on the side of the chamber. Images were taken every 25 min.

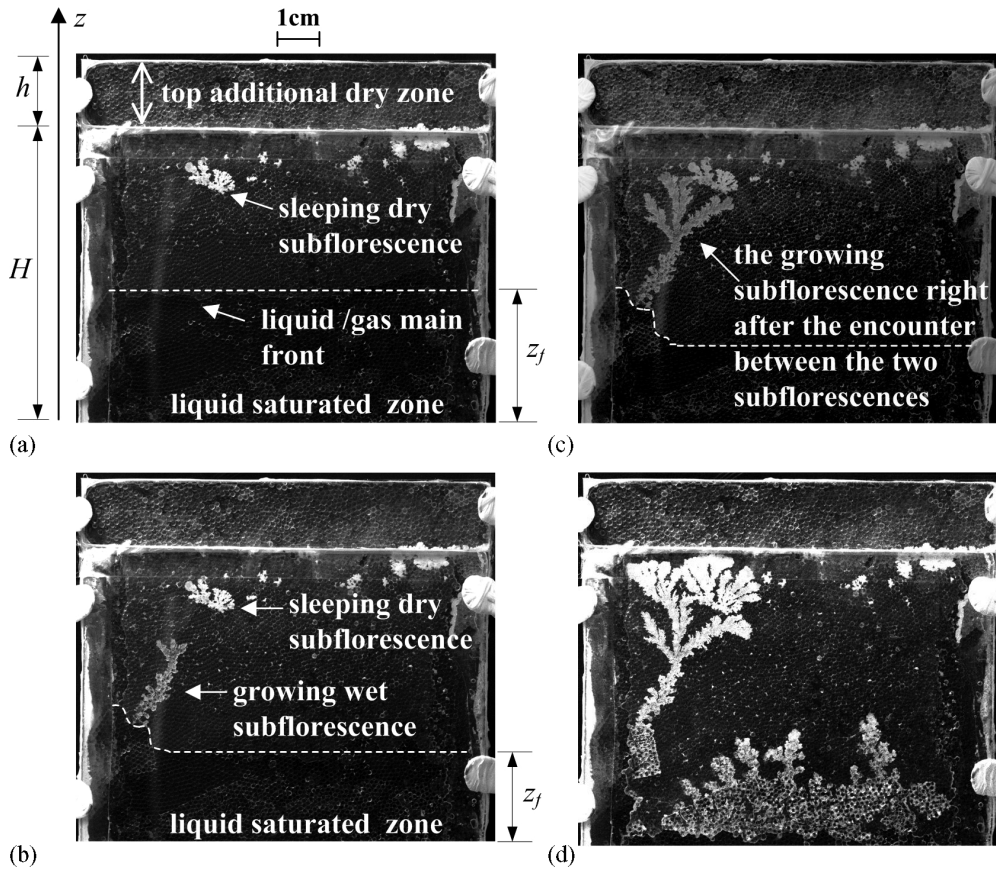---

*Corresponding author: mprat@imft.fr

FIG. 1. Images of model porous medium with subflorescence at different stages of development. The white dashed line approximately marks the separation line between the liquid-saturated zone and the gas-invaded region. Panel (d) shows the system near the end of the drying process. Note the white color of the main subflorescence, indicating that it is now dry, and the major development of new subflorescence at the bottom of the system.

III. RESULTS

The overall duration of the experiment was 67 days and the mass loss of the sample over this duration was 2.5 g. This gives a low mean evaporation flux of $\bar{j} = 4.4 \times 10^{-6}$ kg/m^2/s. As illustrated in Fig. 1, the drying process was characterized by an almost flat traveling front separating the region invaded by the gas phase from the fully saturated liquid zone. This is the pattern expected in a hydrophobic system, e.g., [14]. Moreover, the gravity effects helped to limit the formation of front heterogeneities here [15]. Although the system was hydrophobic, the contact angle ($\sim 107°$–$110°$) was not sufficiently high to prevent the transient trapping of liquid bridges, possibly interconnected [16], in the contacts between beads and between the beads and the plates in the region invaded by the gas phase. The transient existence of the liquid bridges was seen from the formation of small subflorescence spots occurring away from the main front when the liquid bridges evaporated. Interestingly, a larger subflorescence, referred to as the "sleeping" subflorescence in Fig. 1, also formed in the top region of the micromodel. This subflorescence developed in the liquid bridges region without being in direct contact with the main front. This suggests that liquid bridges can occasionally form an interconnected system carrying the dissolved salt between the main front and the growing

subflorescence. After a while, the "sleeping" subflorescence stopped growing and dried. This can be inferred from the change in the subflorescence color from gray when wet to much whiter when dry [see Fig. 1(b) and compare the two main subflorescences]. The explanation is that the chain of liquid bridges feeding the subflorescence no longer forms a hydraulic connection between the subflorescence and the main liquid region after a while. Then the liquid bridges dry out and the subflorescence ceases to grow when all the salt originally present in the liquid bridges has precipitated. Additional details are given in Sec. IV.

Later, when the front had traveled over about two thirds of the micromodel height H, a little protuberance formed along the front as the result of the local pinning of the front on some local defects in the micromodel. This created a local overconcentration in salt, which gave rise to the formation of a major subflorescence, referred to as the wet subflorescence in Fig. 1 and as the main subflorescence in the rest of this paper. The main subflorescence remained attached to the liquid-saturated zone during its growth because of the long pinning of the front where the main subflorescence started growing.

As illustrated in Fig. 1, the first striking observation is that the main subflorescence progressively developed over a macroscopic length, comparable to the size, H, of the
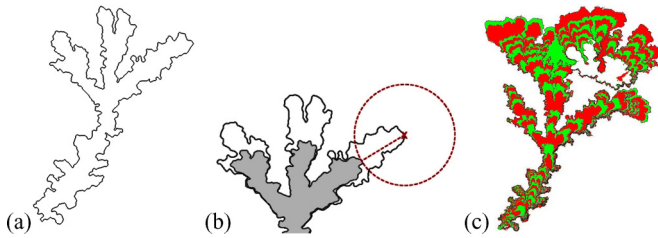
FIG. 2. (Color online) (a) Example of contour of active subflorescence extracted from the raw image after a series of image processing steps; (b) sketch of the method used for determining the local growth rate of subflorescence; (c) visualization of the successive salt deposition layers. Each layer corresponds to the growth occurring during 500 min. The contour of the former "sleeping" dry subflorescence is clearly visible in the upper region.
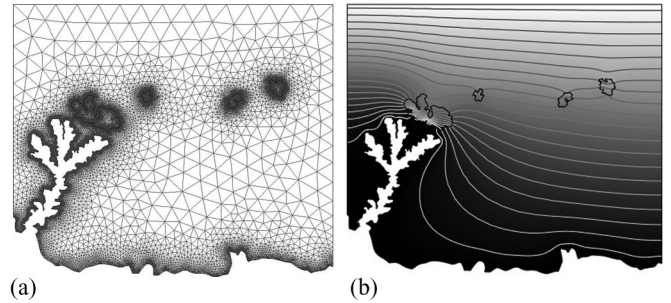

FIG. 3. Two-dimensional finite element computation of evaporation flux along the contour of subflorescence. (a) Finite element mesh; (b) computed water vapor concentration isolines.

micromodel. The second somewhat surprising result is that the growth was not directed toward the liquid solution but in the opposite direction, i.e., towards the open edge of the network and into the gas-invaded region. This was in contrast with experiments in single capillary tubes [17], which have shown that the crystals usually grow into the liquid-saturated region and not in the gas region of the tube.

The color of the main subflorescence was gray when growing, which indicated that the subflorescence was wet. This suggests that the region occupied by the subflorescence was, in fact, porous. As a result, ions could be transported from the solution feeding the subflorescence at its base, within the subflorescence and up to its external boundary, where the salt precipitated and formed a new deposition layer. According to this picture, evaporation at the boundary of the subflorescence is the phenomenon inducing the flow within it and therefore the ion transport.

From a mean field - continuous picture, we should have $u_s = j/\rho_\ell$ along the subflorescence boundary, where u_s is the normal component of the mean velocity in the liquid at the subflorescence boundary, j the local evaporation flux, and ρ_ℓ the solution density. This equation expresses that the evaporation flux is balanced by a liquid flow (due to capillarity) toward the point considered on the subflorescence boundary.

This scenario is supported by what happens when the wet subflorescence reaches the "sleeping" subflorescence. This moment is referred to as the "encounter" of the two subflorescences. When this happens, the "sleeping" subflorescence wakes up and rapidly (in approximately 2 h) becomes gray, which indicates capillary invasion of the sleeping subflorescence by the solution transported through the wet subflorescence, and grows again (see Fig. 1).

To demonstrate that subflorescence growth is indeed driven by evaporation, the evaporation flux along the boundary of the wet (also referred to as active) subflorescence during its growth was computed as follows. First we determined the contour of the active subflorescence during its growth every 500 min (=every 8 h and 20 min). This involved a series of image processing steps using the MATLAB image processing tool box. The details of the image processing will be presented elsewhere. Such a contour is presented in Fig. 2(a).

Then we determined an indicator of local growth rates of the subflorescence as follows. Consider two successive

contours, contours number n and number $n + 1$. N markers were distributed along the contour number $n + 1$ (a contour was formed by a line of pixels and there was one marker at each pixel). Then the distances d_k—where k is the marker index along contour number $n + 1$ (thus k goes from 1 to N), between each marker on contour number $n + 1$ and contour number n—were determined, d_k being the radius of the smallest circle centered on marker number k and intercepting contour number n. The method is sketched in Fig. 2(b). The subflorescence local growth rates were then determined from $r_k = d_k/\delta t$, where δt was the elapsed time between the two contours (thus $\delta t = 500$ min).

The last step consisted in determining the evaporation flux along the contours. The method is illustrated in Fig. 3. Since the growth of the subflorescence was slow, the diffusion problem governing the water vapor concentration c within the gas phase in the micromodel could be considered as quasisteady. The problem to be solved thus read $\nabla \cdot (D\nabla c) = 0$ in Ω_g where Ω_g is the domain occupied by the gas in the system formed by the micromodel and the additional top layer. On top of the domain (at $z = H + h$) we imposed $c = 0$, with a zero flux condition on the lateral edges and $c = 1$ on the subflorescence contour and the liquid-gas main front. For this type of computation, the exact value of D is not important. We took $D = 1$ in the region occupied by the gas and $D = 0.01$ where there were dry subflorescences in Ω_g since the pores were partially blocked by the salt crystals in these regions.

This problem was solved using the commercial simulation software COMSOL MULTIPHYSICS. The numerical solution allowed the local flux along the contour of active subflorescence to be evaluated as $j = D\nabla c \cdot \mathbf{n}$ where $\mathbf{n}$ is the unit vector normal to the contour. This flux was computed where there were markers along contour number $n + 1$, which gave j_k. Then the correlation between the subflorescence local growth rates r_k and local evaporation fluxes j_k was evaluated from the computation of the correlation coefficient,

$$\chi(t) = \frac{\sum_1^N [d_k(t) - \bar{d}_k(t)][j_k(t) - \bar{j}_k(t)]}{\sqrt{\sum_1^N [d_k(t) - \bar{d}_k(t)]^2}\sqrt{\sum_1^N [j_k(t) - \bar{j}_k(t)]^2}},$$

where t is the time, and the overbar, ―, indicates the arithmetic average.

As can be seen from Fig. 4, the correlation coefficient was very high, i.e., close to 1, as expected, demonstrating that
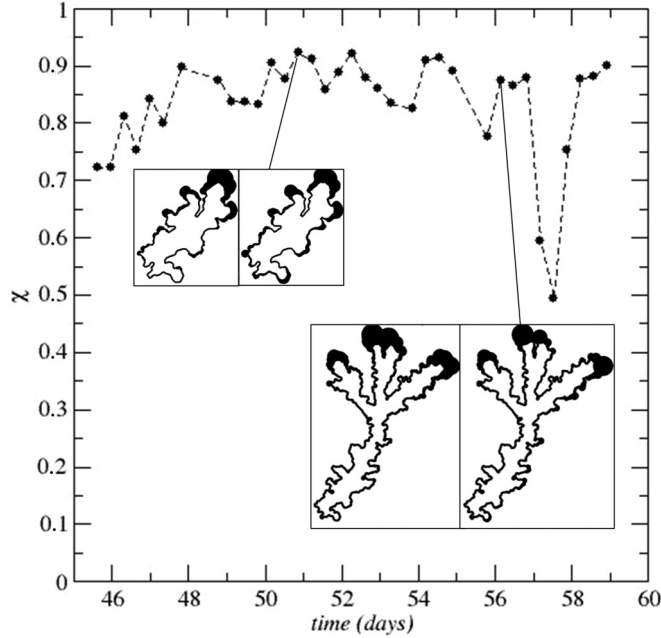
FIG. 4. Correlation coefficient χ between subflorescence local growth rates and local evaporation fluxes at the subflorescence boundary. The drop in the correlation coefficient on the right-hand side of the plot corresponds to the encounter between the two subflorescences (this is so notably because we wrongly imposed $c = 1$ along the contour of the former dry subflorescence even when this subflorescence was not yet reimbibed). The insets show two examples of rescaled distribution of growth rate (figure on the left in each pair of figures) and evaporation flux (figure on the right) along the contour, illustrating the excellent correlation between local growth rates and local fluxes.

the growth of the subflorescence was directly driven by the evaporation process.

IV. DISCUSSION

While the general picture of subflorescence development can be understood from the results reported in the previous sections, two points need further discussion: (i) why the subflorescence growth is not stable, i.e., does not lead to a smooth interface but a ramified structure, and (ii) how ion transport is possible within the subflorescence without pore blocking due to salt precipitation or noticeable dissolution of the subflorescence away from the growing regions. Point (i) can be explained as follows. Due to random heterogeneities, local protrusions form at the evaporating interface, which lead to higher evaporation fluxes, because of the higher local vapor flux (due to the Laplacian). The accompanying salt precipitation creates a fine (water-wet) porous medium, which induces a capillarity-driven flow of water, and the creation of a positive feedback loop that leads to instability, hence the growth of subflorescence. This is essentially the same explanation as given in Ref. [18], where further details can be found, to explain the irregular shape of salt trees growing from a salt solution placed in a Petri dish. Point (ii) is perhaps more puzzling and requires more development.

Since the subflorescence is a porous structure, one can begin with the Darcy's scale equation governing the ion transport within the subflorescence, i.e. [19],

$$\frac{\partial \rho_\ell \varepsilon SC}{\partial t} + \nabla \cdot (\rho_\ell \varepsilon \mathbf{U}_s SC) = \nabla \cdot (\rho_\ell S \varepsilon D_s^* \nabla C) + f, \quad (1)$$

where ρ_ℓ is the density of the solution, ε is the porous medium porosity, S is the liquid saturation in the region occupied by the subflorescence, D_s^* is the effective diffusion coefficient for the dissolved salt, C is the ion mass fraction, $\mathbf{U}_s$ is the average interstitial velocity, and f is the dissolution-precipitation rate per unit volume of porous medium, which is expressed as

$$f = -\varepsilon \rho_{cr} \frac{\partial S_{cr}}{\partial t}, \quad (2)$$

where ρ_{cr} is the density of salt crystal and S_{cr} the crystal saturation (volume fraction of pore space occupied by crystals within the subflorescence). Following [19], f is then expressed as

$$\varepsilon \rho_{cr} \frac{\partial S_{cr}}{\partial t} = K_{cr}(\sigma - 1)^g, \quad (3)$$

where σ is defined by

$$\sigma = \frac{m}{m_{\mathrm{sat}}}. \quad (4)$$

In Eq. (4), m is the molality; m_{sat} is the molality at saturation ($m_{\mathrm{sat}} = 6.1$ molar for NaCl). Expressed in term of mass fraction C, σ reads

$$\sigma = \frac{m}{m_{\mathrm{sat}}} = \frac{C(1 - C_{\mathrm{sat}})}{(1 - C)C_{\mathrm{sat}}}, \quad (5)$$

where the solubility $C_{\mathrm{sat}} = 26.4\%$ for NaCl. According to the data reported in Ref. [19], $g = 1$, $K_{cr} \approx 0.41 \text{ kg/m}^3/\text{s}$ (precipitation) or $0.0128 \text{ kg/m}^3/\text{s}$ (dissolution) in the case of halite (halite is the crystallized form of NaCl), while the supersaturation σ is at most of the order of 1.6, according to [20].

The physical picture is clear. Evaporation at the periphery of efflorescence induces the flow of the solution within the subflorescence. This flow carries the ions toward the evaporative surface where the salt precipitates. As in any reactive flow, an important parameter is the Damköhler number comparing the reaction time scale and the (convective) transport time scale. Here the Damköhler number can be expressed as

$$\mathrm{Da} \approx \frac{K_{cr}[\sigma - 1]L}{\bar{j} C_{\mathrm{sat}}}, \quad (6)$$

where $\bar{j}$ is the mean evaporation flux at the periphery of subflorescence and L is a characteristic length that can be taken as the mean height of subflorescence. Substituting numerical values representative of our experiment in Eq. (6) leads to $\mathrm{Da} \gg 1$. The result is that the reaction is fast compared to transport. Under these circumstances, it can be assumed that the ion mass fraction in the subflorescence is essentially equal to the solubility mass fraction C_{sat}. If the solution was not in equilibrium with the crystallized salt wall, precipitation should lead to pore blockage within the subflorescence or dissolution to shrinking of subflorescence. The fact that the precipitation-dissolution phenomena within the subflorescence are negligible is consistent with the observations since the shape of

subflorescence away from the active evaporation region does not change discernibly during the subflorescence growth.

Unlike the classical case of ion transport in a porous medium, e.g., [8,21], where the key parameter controlling the ion distribution is the Peclet number, which characterizes the competition between convective and diffusive transport, ion transport in the porous subflorescence is thus controlled only by the convective transport ($C \approx C_{\text{sat}}$ within the pores inside the subflorescence, which implies $\nabla C \approx 0$ and thus negligible diffusion transport).

At the bottom of the main subflorescence, the ion supply rate is

$$Q_m = J_s C_{\text{sat}}, \qquad (7)$$

where J_s is the evaporation rate from subflorescence.

Let V be the volume of porous domain occupied by the solution feeding the subflorescence at its base. A simple mass balance gives

$$\rho_\ell \varepsilon \frac{dV}{dt} = -J_s - J_f, \qquad (8)$$

where J_f is the evaporation rate from the fraction of the boundary of this region not in contact with subflorescence.

Since the ion leaves this shrinking region only through the subflorescence, the ion mass balance for this region is

$$\rho_\ell \varepsilon \frac{d\bar{C}V}{dt} = -C_{\text{sat}} J_s, \qquad (9)$$

where $\bar{C}$ denotes the average ion mass fraction in this region.

From the visual inspection of the main subflorescence growth, one can make the rough approximation that the subflorescence growth is rapid compared to the change in the volume V, and so $V \approx$ cst during the subflorescence growth. Then Eq. (9) yields

$$\rho_\ell \varepsilon V \frac{d\bar{C}}{dt} \approx -C_{\text{sat}} J_s, \qquad (10)$$

which indicates that the average ion mass fraction in volume V decreases during the subflorescence growth. Thus the subflorescence growth tends to desalinate the solution feeding it at its base.

This is consistent with the observations that show growth of new subflorescence structures [visible in the lower region of the micromodel in Fig. 1(d)] from shrinking volume V, starting only some time after the saturated region at the bottom of our micromodel has detached from the main subflorescence.

This also indicates that the main subflorescence stops growing not because of precipitation phenomena blocking the pores but because it stops being fed by the solution at its base when the subflorescence ceases to be in hydraulic contact with the solution as the result of invasion front receding due to evaporation.

The same lines of argument can be developed to explain how the subflorescence referred to as the "sleeping" subflorescence "goes to sleep." When the subflorescence ceases to be hydraulically connected to the solution, it forms a liquid-saturated porous structure in equilibrium with the solution contained in it ($C \approx C_{\text{sat}}$ throughout the pore space). Then this subflorescence dries as, once again, the ions are transported to the evaporation active surface of the subflorescence where the salt precipitates
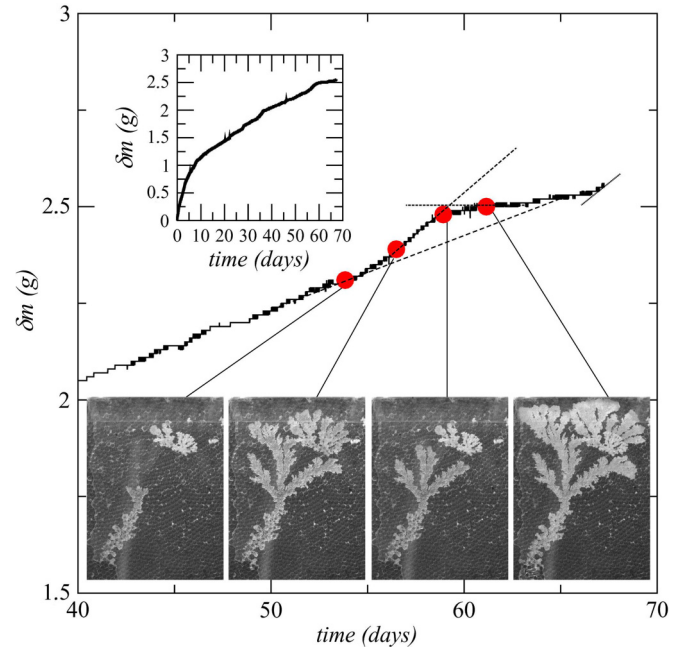

FIG. 5. (Color online) Evaporated mass of water versus time (inset). The main figure shows the variation of the evaporated mass of water during the period of growth of the main subflorescence. The dashed lines are guides to the eye materializing the change in the evaporation rate (slope of lines) when the main subflorescence develops and dries out (after union with the sleeping subflorescence).

to form new porous salt layers. This scenario is completely in line with observations which show preferential growth of this subflorescence at its upper part where evaporation fluxes are obviously greater and there is no pore blockage since the subflorescence resumes its growth when rewetted later as the result of the development of the main subflorescence.

From the above analysis, it is expected that the development of subflorescence must have an impact on the overall drying rate. The evaporation rate is roughly inversely proportional to the distance between the menisci inside the porous medium and the inlet of the porous medium. The result of subflorescence growth is to bring menisci much closer to the micromodel inlet and thus to reduce the mean distance between the menisci present in the system and the inlet. The conclusion is that the evaporation rate must increase with the development of subflorescence. This can be clearly seen from Fig. 5, which shows the evolution of the evaporated mass of water with time during the growth of the main subflorescence. The evaporation rate increases markedly during the growth of the main subflorescence and its subsequent encounter with the sleeping subflorescence, which causes the rewetting of the latter and subsequent significant subflorescence growth in the inlet region of the micromodel. Then the evaporation rate decreases consistently and significantly as the system formed by the union of the main subflorescence and the former sleeping subflorescence dries out (which corresponds to the plateau on the right in Fig. 5). The dry subflorescence forms a region of lower porosity and thus of less conductance for the diffusive transport of the vapor across the dry region of the model porous medium. This additional resistance combined with the fact that the gas-liquid front has receded into the

system during the growth of the subflorescence explains the reduced evaporation rate after the drying of the main subflorescence. The final increase of the evaporation rate that can be discerned on the far right of the mass versus time curve in Fig. 5 is attributed to the growth of the bottom subflorescence clearly visible in the lower region of the micromodel in Fig. 1(d).

V. CONCLUSION

This study shows that development of subflorescence driven by evaporation can occur over macroscopic distances within a porous medium. The analysis indicates that most of the salt structure is in equilibrium with the solution traveling through it, which explains why the structure can continue to grow without significant pore blockage by precipitation or dissolution of the structure away from the evaporative surface. Here the precipitation kinetics does not play any role in the subflorescence growth kinetics, which is controlled by the transport of ions to the subflorescence evaporative surface and thus the evaporation flux distribution and its evolution at the periphery of the subflorescence. This is so because the precipitation time scale is much smaller than the ion transport time scale.

This study also suggests that a major development of subflorescence in a porous medium could be detected from the variation of the evaporation rate, which tends to increase as the result of subflorescence development. This is in contrast with classical drying kinetics under stationary external drying conditions, which never show an increase in the evaporation rate.

This study is of broader interest in relation with the widely studied domain of Laplacian growth [22]. Here, the growth results form an interesting coupling between evaporation (determined from the solution of the Laplace equation), capillarity (which induces the liquid flow in the subflorescence and thus the ion transport), ion transport, and crystallization. The interplay between these phenomena is likely to lead to various patterns and this clearly deserves further studies. This is supported by our recent study on efflorescence [6,10]. From the results reported in Refs. [6,10], we surmise that major subflorescence developments such as the ones reported in the present paper can be expected for sufficiently slow evaporation rates and systems with relatively large pores. When these conditions are not met, subflorescence development could be inhibited by limited solution transport capacity toward its boundary due to viscous effects and/or possibly to salt precipitation (when the evaporation rate is sufficiently high for the ion transport time scale not to be considered large compared with the precipitation time scale; it can also be hypothesized that the probability of blocking pores would increase with decreasing pore size), leading to possibly different subflorescence patterns. This is supported by the results reported in Refs. [23,24] showing decreasing rates of drying for salt-laden real materials. The next step is therefore to investigate the influence of evaporation rate and pore size on subflorescence growth.

[1] U. Nachshon, N. Weisbrod, M. I. Dragila, and A. Grader, Water Resour. Res. **47**, W03513 (2011).

[2] Y. Peysson, Eur. Phys. J. Appl. Phys. **60** 24206 (2012).

[3] A. Goudie and H. Viles, *Salt Weathering Hazards* (Wiley, Chichester, UK, 1997).

[4] G. W. Scherer, Cem. Concr. Res. **34**, 1613 (2004); O. Coussy, J. Mech. Phys. Solids **54**, 1517 (2006).

[5] S. Veran-Tissoires, M. Marcoux, and M. Prat, Phys. Rev. Lett. **108**, 054502 (2012); Europhys. Lett. **98**, 34005 (2012).

[6] H. Eloukabi, N. Sghaier, S. Ben Nasrallah, and M. Prat, Int. J. Heat Mass Transfer **56**, 80 (2013).

[7] M. Norouzi Rad, N. Shokri, and M. Sahimi, Phys. Rev. E **88**, 032404 (2013); N. Shokri, Phys. Fluids **26**, 012106 (2014).

[8] F. Hidri, N. Sghaier, H. Eloukabi, M. Prat, and S. Ben Nasrallah, Phys. Fluids **25**, 127101 (2013).

[9] S. Gupta, H. Huinink, M. Prat, L. Pel, and K. Kopinga, Chem. Eng. Sci. **109**, 204 (2014).

[10] S. Veran-Tissoires and M. Prat, J. Fluid Mech. **749**, 701 (2014).

[11] N. Sghaier, M. Prat, and S. Ben Nasrallah, Chem. Eng. J. **122**, 47 (2006).

[12] F. Chauvet, P. Duru, S. Geoffroy, and M. Prat, Phys. Rev. Lett. **103**, 124502 (2009).

[13] N. Sghaier, Ph.D. thesis, Institut National Polytechnique de Toulouse, 2006.

[14] O. Chapuis and M. Prat, Phys. Rev. E **75**, 046311 (2007); H. Chraibi, M. Prat, and O. Chapuis, *ibid.* **79**, 026313 (2009).

[15] M. Prat and F. Bouleux, Phys. Rev. E **60**, 5647 (1999).

[16] M. Sheel, R. Seeman, M. Brinkmann, M. Di. Michiel, A. Sheppard, and S. Herminghaus, J. Phys.: Condens. Matter **20**, 494236 (2008).

[17] N. Shahidzadeh and J. Desarnaud, Eur. Phys. J. Appl. Phys. **60**, 24205 (2012).

[18] R. Du and H. A. Stone, Phys. Rev. E **53**, 1994 (1996).

[19] H. Derluyn, P. Moonen, and J. Carmeliet, J. Mech. Phys. Solids **63**, 242 (2014).

[20] J. Desarnaud, H. Derluyn, J. Carmeliet, D. Bonn, and N. Shahidzadeh, J. Phys. Chem. Lett. **5**, 890 (2014).

[21] Y. T. Puyate, C. J. Lawrence, N. R. Buenfeld, and I. M. McLoughlin, Phys. Fluids **10**, 566 (1998); H. P. Huinink, L. Pel, and M. A. J. Michels, *ibid.* **14**, 1389 (2002); L. Guglielmini, A. Gontcharov, A. J. Aldykiewicz, and H. A. Stone, *ibid.* **20**, 077101 (2008).

[22] P. Meakin, *Fractals, Scaling and Growth Far from Equilibrium* (Cambridge University Press, Cambridge, 1998).

[23] T. D. Goncalves, L. Pel, and J. D. Rodrigues, Environ. Geol. **52**, 293 (2007).

[24] R. M. Espinosa-Marzal and G. W. Scherer, Environ. Earth Sci. **69**, 2657 (2013).